Non-Radiative Step Facets in Semiconductor Nanowires

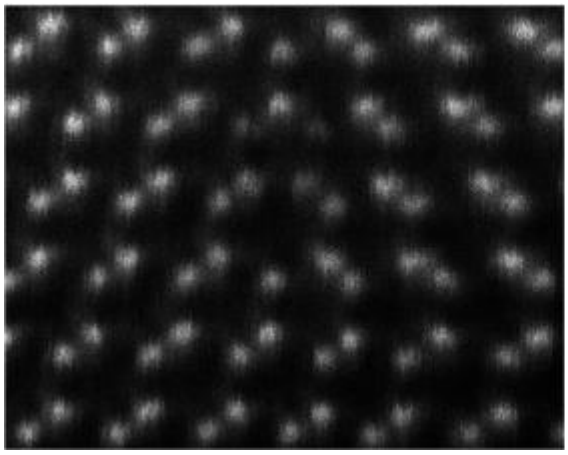

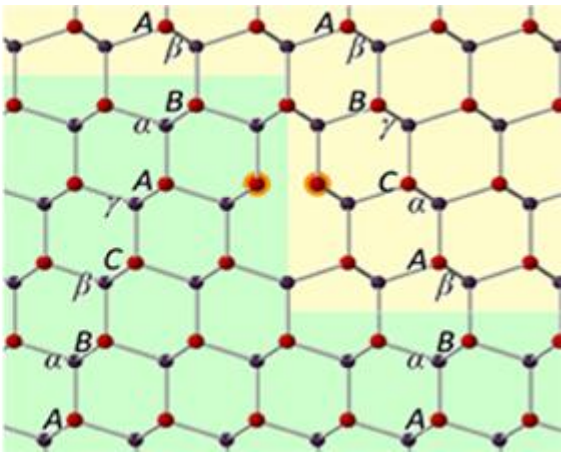

Non-Radiative Step Facets in Semiconductor Nanowires

Ana M. Sanchez[§*], Yunyan Zhang[†] Edward W. Tait[¥], Nicholas D. M. Hine[§], Huiyun Liu[†] and Richard Beanland[§*],

[§] Department of Physics, University of Warwick, Coventry CV4 7AL, United Kingdom

[†]Department of Electronic and Electrical Engineering, University College London, Torrington Place, London WC1E 7JE, United Kingdom

[¥]TCM Group, Cavendish Laboratory, 19 JJ Thomson Avenue, Cambridge, CB3 0HE, United Kingdom.

Abstract:

One of the main advantages of nanowires for functional applications is their high perfection, which results from surface image forces that act on line defects such as dislocations, rendering them unstable and driving them out of the crystal. Here we show that there is a class of step facets that are stable in nanowires, with no long-range strain field or dislocation character. In zinc-blende semiconductors, they take the form of Σ3 (112) facets with heights constrained to be a multiple of three {111} monolayers. Density functional theory calculations show that they act as non-radiative recombination centres and have deleterious effects on nanowire properties. We present experimental observations of these defects on twin boundaries and twins that terminate inside GaAsP nanowires and find that they are indeed always multiples of three monolayers in height. Strategies to use the three-monolayer rule during growth to prevent their formation are discussed.

KEYWORDS: Nanowire, defects, STEM, DFT, step facets.

One dimensional nanostructures, commonly known as nanowires (NWs), are of continued interest for next-generation optoelectronics,[1, 2] sensors, photovoltaics and many other applications.[3] One of the principal reasons for this interest is that nanowire crystal structure is essentially independent of the substrate, removing the severe constraints of lattice parameter-matching that so limits the range of epitaxial layers on bulk substrates.[4] Additionally, the rod, ribbon and shell geometries available within a nanowire provide new ways to manipulate quantum confinement of charge carriers and optical density that may have advantages over more traditional approaches.[1, 5] The enormous range of possibilities and heterostructures is only beginning to be investigated and may be expected to produce useful outputs such as integration of compound semiconductor optoelectronics with silicon microelectronics.[1, 3]

One of the great benefits of the NW geometry is the lack of any stable location for a dislocation in the unstrained structure, apart from Eshelby's well-known metastable solution for a screw dislocation along its axis if the NW is allowed to twist.[6, 7] Any other dislocation in a NW experiences an attractive force to the surface, and if it is mobile it will move out of the NW. Although immobile and geometrically necessary dislocations (e.g. in high-angle grain boundaries[8]) may exist in NWs, careful growth can prevent their formation and thus line defects with long-range strain fields are essentially absent. This high degree of perfection removes one of the principal causes of non-radiative recombination that affects lattice mismatched semiconductors grown as epitaxial layers, giving NWs a significant advantage for materials and compositions that are otherwise inaccessible. However, planar defects such as stacking faults and twin boundaries, as well as changes in bulk structure (i.e. polytypes), are commonly reported.[3, 9-12] Here, we examine {211} facets on {111} twin boundaries in self-catalysed (Ga droplet) $GaAs_{0.95}P_{0.05}$ zinc-blende (ZB) NWs by molecular beam epitaxy. We find that such facets are stable inside the NWs if they have heights that are multiples of 3 monolayers, and that they will act as non-radiative recombination centres. All experimental observations agree with this three-monolayer rule.

The self-catalyzed GaAs(P) nanowires were grown directly on p-type Si(111) substrates by solid-source III−V molecular beam epitaxy (MBE). GaAs NWs were grown with a Ga beam equivalent pressure, V/III flux ratio, substrate temperature, growth duration and nominal doping concentration

(characterized in thin film growth) of 8.41×10^{-8} Torr, 44, ~630°C, 1 hour and $0\sim1.28\times10^{19}/cm^3$, respectively. The droplet consumption was conducted by keeping wafer under only As flux of $\sim6\times10^{-7}$ Torr with rapid temperature decrease. GaAsP NWs were grown with a Ga beam equivalent pressure, V/III flux ratio, P/(As+P) flux ratio, substrate temperature, duration and nominal doping concentration of 8.41×10^{-8} Torr, 40, 0.16, ~640 °C, 1 hour, and $8.9\times10^{18}/cm^3$, respectively. The patterned Si (111) substrates were prepared using nano-imprint lithography. The NWs were grown with a Ga flux of 1.6×10−7 Torr, V/III flux ratios between 3 and 20, growth temperature of ~630°C and a P/(P+As) flux ratio of 12% throughout the growth duration of 45 minutes. Detailed information can be found in [13-15 16, 17]. Simple scraping of the NWs onto a lacy carbon support was used to prepare transmission electron microscopy (TEM) specimens. STEM analysis was performed on a doubly-corrected ARM200F microscope operating at 200 kV. ADF STEM images were obtained using a JEOL annular field detector using a fine-imaging probe, at a probe current of approximately 23 pA with a convergence semi-angle of ~25 mrad. DFT Calculations: An energy cut-off of 700 eV was employed along with the default CASTEP[18] on-the-fly pseudopotentials and the PBE functional[19]. The original 12 atom cell was subject to both position and cell optimisation. The cell parameters were optimised until the maximum stress tensor component was less than 0.1GPa. For the 288-atom models (see Fig. S3a) a Monkhorst-Pack *k*-point grid of 1x5x1 was used. The models were optimised using the BFGS algorithm until residual forces were less than 0.05 eV/A. Projected densities of state were computed for the final relaxed geometry. Conversion of raw output into data suitable for plotting was accomplished using the OptaDoS tool [5]. A fixed width smearing scheme was used, with a smearing width setting of 0.05 eV. The DoS was sampled at 0.005 eV intervals. For calculating the projections, the step regions were defined as those containing the atoms within the orthorhombic 12-atom GaAs cell on either side of the step.

The vapour-liquid-solid (VLS) technique uses a liquid metal droplet to absorb vapour until it is saturated, whereupon material precipitates from the droplet onto the NW, almost always in the form of a close-packed atomic plane that adds to the crystal and pushes the droplet one monolayer further from the substrate.[12, 20] In {111} zinc-blende III-V NWs, twins can be extremely common.[9] The energy barrier for nucleation of a monolayer with twinned orientation on a {111} facet is very low,

leading to their formation during crystal growth. They usually extend across the full width of the NW (Fig. 1) and polarity is maintained across the boundary as observed in Figs. 1b and c (an ortho twin,[21] see Supplementary Information 1).

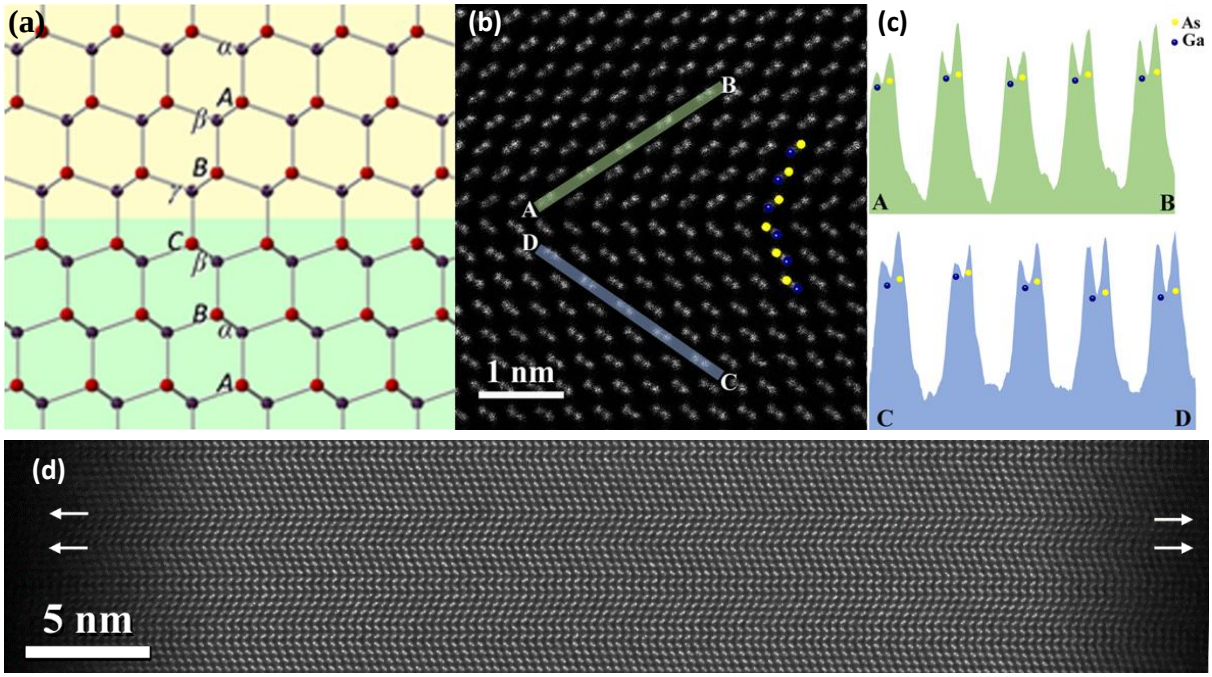

Figure 1. Scanning Transmission Electron Microscopy (STEM) analysis of an ortho twin boundary. (**a)** Schematic of an ortho twin boundary, with group III atoms, Ga, blue and group V, $As_{0.95}+P_{0.05}$, red. **(b)** Atomic resolution ADF-STEM image of a twin boundary in a $GaAs_{0.95}P_{0.05}$ NW. **(c)** Line profiles AB and CD showing the same <111>B polarity on both sides of the boundary. Group III atoms have a mean atomic number of 31, while group V atoms have a mean atomic number of 32, giving a nominal difference in contrast of ~6%. In common with other groups, we find that the NWs grow along (111)B.[9] **(d)** Lower magnification image showing that the twin boundaries (indicated with white arrows) extend across the full width of the NW. The growth direction is vertical.

Since there is no disruption to tetrahedral bonding, twin boundaries appear to be relatively benign; they have little effect on bulk band structure, although they may alter the recombination lifetime of

some excitons[22] and reduce charge carrier mobilities[23]. It has been proposed that they are responsible for enhanced recombination at the NW surfaces[24], although surface recombination is a well-known problem that is addressed by core-shell structures to confine carriers to the NW core.[17] However, while a planar twin boundary may not affect electronic properties significantly, a step in the boundary may have more disruptive and unwanted properties.

A monolayer step in a twin boundary interface has an associated dislocation, well-known as a glissile 'twinning' dislocation with Burgers vector $1/6\langle 11\bar{2}\rangle$ in the face centred cubic structure. The dislocation and monolayer step are inextricably linked; if a monolayer step is present, there must be a $1/6\langle 11\bar{2}\rangle$ interfacial dislocation present and vice-versa. Such a dislocation, if it did exist in a NW, would glide to the free surfaces at the edges due to image forces and exit the NW. Nevertheless, not all interfacial steps have dislocation character. In general, an interfacial step will have zero Burgers vector if it satisfies the condition[25]

$$W_\lambda = PW_\mu^{-1}P^{-1} \qquad (1)$$

where W_λ and W_μ describe the steps on the matching surfaces of the crystals on either side of the boundary, and P the coordinate transformation from one crystal to the other (Supplementary Information 2). Interestingly, an interfacial step has topological properties similar to those of other line defects, i.e. it cannot terminate inside the NW but must either form a closed loop or continue to the surface of the crystal. It can be described by a step vector, **t**, which is conserved in the same way as a Burgers vector. Equation (1) applies to all crystal structures and gives the condition for stability of interfacial steps in twin boundaries in any type of nanowire. In twin interfaces in ZB crystals, equation (1) is only satisfied by steps that are described by a step vector **t** = [111], three monolayers in height, or multiples of the same.

Now, a step which satisfies Eq. 1 may not have a Burgers vector, but it is not perfect crystal either. Figure 2a shows such a step, imaged with atomic resolution ADF-STEM. In agreement with the 'three-monolayer rule' above, it has a height of six monolayers. Figure 2b is a magnified view of the first three-monolayer step. Interestingly, if polarity is maintained across the (111) boundaries on either side of the step, the material on opposite sides of the interfacial plane are related by a mirror,

and it is a $(11\bar{2})$ para twin (Fig. 2c). Measurement of the intensities of the III- and V-sublattices shows this indeed to be the case (Fig. 2d). The Σ3 $(11\bar{2})$ interface is composed of 5- and 7-membered rings[11] that contain under-bonded and over-bonded atoms. In particular, the central pair of As atoms highlighted in Fig. 2c are under-bonded and have As-As bonds in our structural model; by analogy with a dislocation this is known as an As-core Σ3 $(11\bar{2})$ boundary. An 'up' step must have a structure of polarity opposite to the 'down' step shown in Fig. 2c, and is a Ga-core Σ3 $(11\bar{2})$ boundary. The Σ3 $(11\bar{2})$ boundary is extremely common in bulk polycrystalline semiconductors and has been studied in diamond,[26] silicon,[27-30] III-Vs[31] and II-VIs.[32, 33] A variety of reconstructions have been observed and/or calculated for Σ3 $(11\bar{2})$ boundaries in these different materials; the boundary also been proposed as a preferential site for impurity atoms.[30, 32-34] Some effort has been made to understand and passivate their detrimental activity in solar cell materials.[32, 34]. Facets such as that shown in Fig. 2 can move without the need for any long-range diffusive flux, and may do so by breaking and reforming bonds in a similar manner to an undissociated 60° glide dislocation. In the absence of any long-range strain field to provide a driving force and a reported activation energy of ~1 eV for glide in GaAs[35] this implies that they are sessile and essentially fixed in place. Thus, given that these step facets are stable in NWs it is important to examine their likely impact on nanowire functionality.

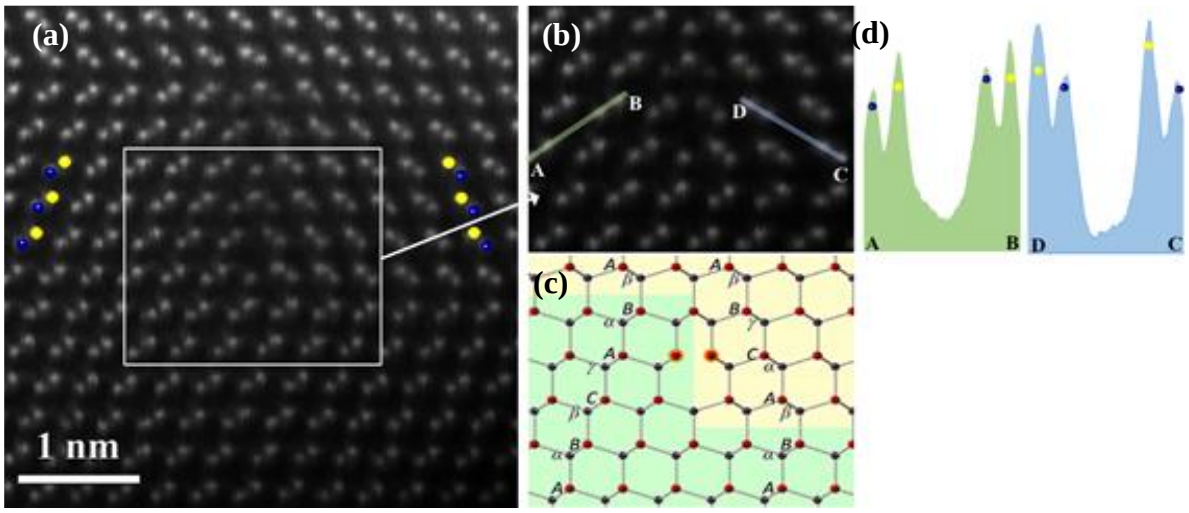

Figure 2. Scanning Transmission Electron Microscopy (STEM) analysis of coherent Σ=3 $(1\bar{1}2)$ para twin. **(a)** A step in a (111) ortho twin boundary that forms a coherent Σ=3 $(1\bar{1}2)$ para twin

facet six monolayers high. (**b)** Magnified image of the area inside the white rectangle. **(c)** Schematic of a three monolayer step, showing that the polarity across the {111} plane is preserved on either side of the step and that atoms on opposite sides of the $(1\bar{1}2)$ facet are related by a mirror. The highlighted As atoms form an As-As bond in the DFT model, while the As and Ga atoms on the boundary plane become five-fold and three-fold coordinated, respectively (See Fig. S6). (**d**) Line profiles AB and CD showing the para twin character of the Σ=3 $(1\bar{1}2)$ boundary.

We use density functional theory (DFT)[36, 37] calculations to investigate the possible structural models of the 6-monolayer form of the Σ3 $(11\bar{2})$ step facet and the impact it would have on electronic properties. The small fraction of phosphorous in the examined NWs was omitted from this model since it will only have a second order effect on electronic structure. Initial models of the boundaries and steps were produced by tiling an orthorhombic 12-atom GaAs cell, and a twinned cell rotated 180° about an appropriately chosen axis. A 288-atom simulation cell was constructed (Fig. S3a) containing an included 4x2 region of the rotated structural unit, surrounded by a 4x2-cell region of the original structure along the *x*-direction and an 8x1-cell region of the original structure along the *y*-direction. This model contains two steps to enable periodic boundary conditions, with one step containing an As-As core and one containing a Ga-Ga core, separated by 28 Å. For comparison, a 288-atom bulk cell and a 288-atom region of ortho twin boundary were produced. These models were then geometrically relaxed, and projected Densities of States (pDOS) were calculated for each region of each model. The model required Ga-Ga bonds in the Ga-core step, and after relaxation produces one over-coordinated As atom and one under-coordinated Ga atom, both lying on the symmetry plane associated with the step (Fig. S6). Likewise, there are As-As bonds in the As-core step, and one over-coordinated Ga and one under-coordinated As atom. Such coordination changes are known from other theoretical studies on monoatomic and III-V semiconductors to contribute to the formation of localised gap states.[26, 30, 38-40]

The 6-layer step model relaxes to a geometry in very good agreement with the STEM images (Figure S5). No asymmetry in structure or rigid-body shift developed at the (211) facet, even though no

constraints were in place that would prevent these effects. All Ga-As bond lengths in the vicinity of the step relax to no more than 7% extension or 3% compression compared to DFT bulk bond length (2.49 Å), while the As-As and Ga-Ga bonds within the boundary cores are within 2% of the DFT bulk bond length.

Figure 3 shows the total density of states for the three cells. The bulk cell (dark red) exhibits a band gap of 0.4 eV, which is significantly underestimated as is standard for DFT calculations with semi-local functionals. In this situation we are interested in changes in band gap due to the step model, rather than the value itself. For the ideal ortho twin-boundary model (green), with no steps, there is a small reduction of the overall gap (to 0.35 eV). By contrast, for the 6-layer step model (blue), the band gap is effectively closed by the mid-gap states, resulting in a small but finite density of states within the region of the original gap. In both cases, the step regions are associated with band-bending: the pDOS of the As-As step region (inset, blue) is shifted upwards in energy, while that of the Ga-Ga step region (inset, orange) is shifted downwards. In agreement with previous studies of the extended grain boundary corresponding to this step,[26, 30, 38-40] there are also clear signs of localised states associated with coordination changes, which lie in the energy range corresponding to the mid-gap region of the bulk structure. These contribute to closing the overall gap of the system. Investigation of the distribution of the Kohn-Sham eigenstates around the Fermi level indicate that these states are relatively well-localised to the step region, although in this finite periodic model there is some hybridisation between states localised at the Ga-Ga and As-As steps.

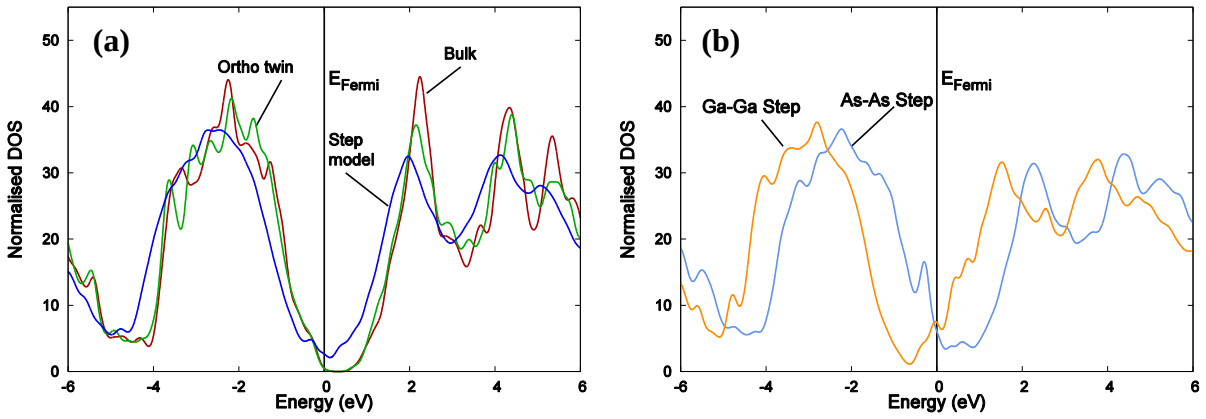

Figure 3. Calculated densities of states for the model systems considered. **(a)** The step model (blue) shows a closed band gap with respect to the perfect (red) and ideal 211 boundary (green) models. This closure is due localised band banding created by the step structures. **(b)** Projected density of states plots for the regions in the vicinity of the two step structures. Bands near the Ga-Ga step structure (Orange) are shifted down in energy with respect to the bulk, whereas those near the As-As step (blue) are shifted up in energy.

This strong modification of the electronic structure in the step regions suggests that the steps would constitute strong charge recombination centres if they were present within a nanowire, even though they do not possess dislocation character. This would be expected to result in a strong influence on optoelectronic properties. It is also likely, based on the metallic character of these boundaries, that they would lead to shorting of charge separation within core-shell structures.

The three-monolayer rule applies not only to steps in {111} boundaries, but also to twins that terminate within the wire and these will have similar electronic properties. An example of such a twin that terminates within the NW is shown in Fig. 4, which is (as expected) three monolayers in thickness. In this case however, the atomic arrangement at the end of the twin initially appears not to be as straightforward as the step shown in Fig. 2. Examining the contrast in detail, Ga atoms can be clearly observed in the lowest of the three layers (bottom atoms) while the As atoms immediately above them appear indistinct and blurred. Similarly, in the 3rd layer, only the As atoms are well defined (top atoms), while in the central 2nd layer neither the Ga or As are clearly distinct in the area close to the end of the twin (see magnified image in Fig. 4b). This contrast can be explained if the end facet of the twin is not parallel to the point of view. In fact, we find that the image is consistent with a twin terminated by a $\Sigma 3$ $(11\bar{2})$ facet that lies at 60° (Supplementary 3) to the electron beam. A $[1\bar{1}0]$ projection of a region containing both twin and matrix structure has an atomic structure that matches exactly the experimentally observed contrast. We have also observed similar structures in other III-V NWs (Supplementary 4).

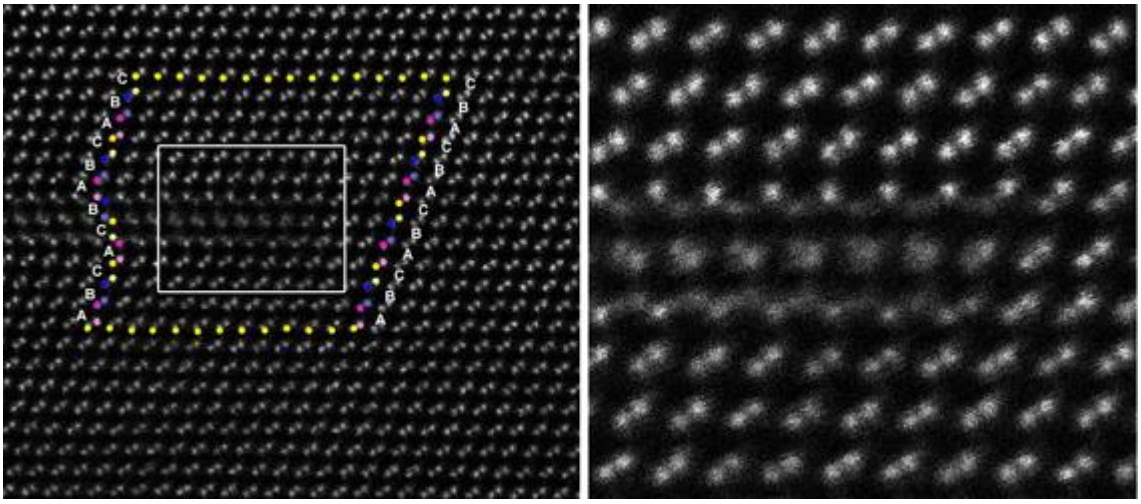

Figure 4. Boundary terminating in the Nanowire. **(a)** Three-monolayer steps in {111} twin boundary terminating within the nanowire. **(b)** magnified image of the area enclosed in the white rectangle

Since these step facets are likely to be problematic for functional NWs, methods to avoid them need to be considered. Importantly, the lack of any long-range strain field for these step facets renders them difficult to detect. In low magnification TEM images, unlike dislocations, they give no additional contrast and are easily missed. We have no easy way to estimate their frequency in NWs apart from high-resolution imaging; furthermore, they are only clearly visible when viewed along one of the three possible <110> directions. Careful examination of the NWs in this study (each of which was approx. 2μm in length) suggests that their density is roughly one step facet in every two or three NWs; nevertheless, substantial variation in their density may be present depending upon growth conditions. While this density is difficult and time-consuming to detect by TEM, it may still be sufficient to affect NW properties; the only sure way to prevent them is to produce NWs that are completely twin-free. It has been proposed that the perfection of the twins in III-V NWs implies that each new monolayer added to the crystal during growth has only one nucleation site.[9] Obviously, if there is only one nucleation site where a new monolayer begins to be deposited from the liquid droplet, that monolayer will have the same orientation across the full width of the NW and no step can form. However, the restrictions on stability imposed by the three-monolayer rule may also play a crucial role. In-situ studies have shown complex time-dependent faceting at the solid-liquid interface

in the growth of ZB nanowires, which implies there can often be multiple nucleation sites at the droplet-NW interface.[12, 41] In such a case, as shown schematically in Fig. 5a, it is conceivable that one of the new monolayers is an ortho twin and the other part is not. Once the two halves of the new monolayer meet (Fig. 5b), a discontinuity is formed. It is possible that the energy of this discontinuity may already be sufficient to cause it to move to the edge of the monolayer at this point, but in any case once one variant begins to overgrow the other a twinning dislocation must form (Fig. 5c) and surface forces will act to move it to the edge of the nanowire. Thus, it may be that many steps that do form in (111) twin interfaces during growth will be eliminated before they can become stable. The two variants will only be able to coexist if they both manage to reach heights of at least three monolayers before they meet. Once they are overgrown a $\Sigma 3\ (11\bar{2})$ boundary will be present between them that will ideally adjust itself to be a dislocation-free multiple of three monolayers in height, as observed here in Figs. 2 and 4.

Three-monolayer steps may also be avoided by maintaining small lateral nanowire dimensions (which is often desired for other reasons as well) and restricting the growth area where nuclei can form. This will reduce the probability that two separate nucleation sites both reach a height of more than three monolayers before they meet.

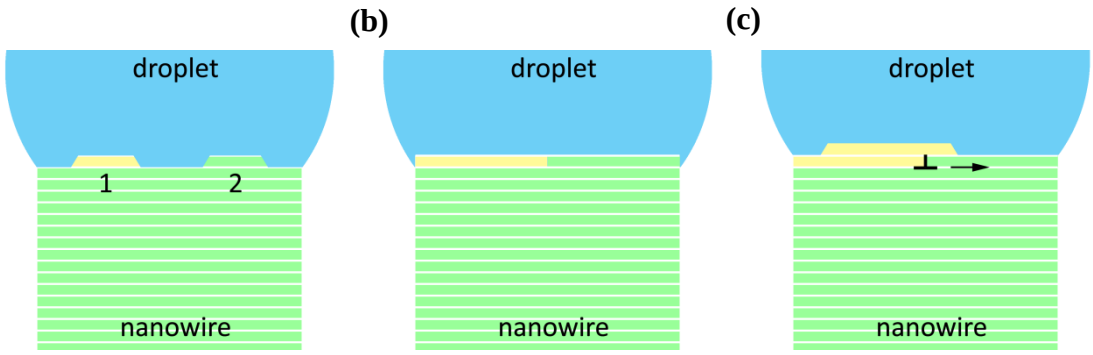

Figure 5. Suggested mechanism of elimination of a monolayer height twin step during NW growth. **(a)** A new (111) monolayer begins to be deposited from two different nucleation sites, one of which is in twin orientation with respect to the underlying material. **(b)** when the two monolayers meet, they form a discontinuity. **(c)** overgrowth of this boundary by a new monolayer would produce a

twinning dislocation that would immediately move to the edge of the NW.

Finally, we note that similar defects may form in nanowires, nanoparticles and indeed 2D materials, in any crystal structure, and each will have their own rules for step height in accordance with Eq. (1). Without a strain field that allows them to be easily detected, they may be a common, but hitherto overlooked, feature of crystals with small sizes in one, two or three dimensions.

In summary, we have considered steps in twin boundaries as a form of defect and shown that in zinc-blende semiconductor NWs they will act as non-radiative recombination centres. They have topological properties similar to those of dislocations, but no long-range strain field. This makes them difficult to detect; their density in typical nanowires is currently unknown. We give a general rule that predicts when they are stable in any crystal with small dimensions. In III-V ZB NWs, this gives a *'three-monolayer rule'* that must be obeyed by $\Sigma 3$ $(11\bar{2})$ twin boundaries in zinc-blende III-V nanowires and all our experimental observations are in agreement with this constraint.

ASSOCIATED CONTENT

Supporting information

A description of the ortho- and para- twins and the bicrystallography approach to describe the three monolayer steps. Two different examples of a twin terminated by a $\Sigma 3$ $(11\bar{2})$ facet have been also introduced to understand the contrast observed in certain areas of the NWs. Additional examples of twins terminating in the interior of the NW and obeying the three monolayer rule are also given.

AUTHOR INFORMATION

Corresponding Authors

*E−mail: a.m.sanchez@warwick.ac.uk, r.beanland@warwick.ac.uk,

Author contributions

AMS, and RB performed aberration corrected STEM with samples prepared by prepared by YZ and HL. EWT and NDMH set up, executed and analyzed the DFT calculations.

RB and AS wrote the paper with input from all authors.

ACKNOWLEDGMENTS

This work is supported by the Leverhulme Trust (HL) and EPSRC (EP/P000916/1, EP/P000886/1). EWT was supported by the EPSRC Cambridge NanoDTC, EP/G037221/1. Computing facilities were provided by the Centre for Scientific Computing at the University of Warwick. Supporting data may be obtained from http://wrap.warwick.ac.uk/86316

COMPETING FINANCIAL INTERESTS

The authors declare no competing financial interests.

REFERENCES

1. Yan, R. X.; Gargas, D.; Yang, P. D. *Nat. Photonics* **2009,** 3, (10), 569-576.
2. Zhang, Y. Y.; Wu, J.; Aagesen, M.; Liu, H. Y. *J. Phys. D-Appl. Phys.* **2015,** 48, (46), 29.
3. Dasgupta, N. P.; Sun, J. W.; Liu, C.; Brittman, S.; Andrews, S. C.; Lim, J.; Gao, H. W.; Yan, R. X.; Yang, P. D. *Adv. Mater.* **2014,** 26, (14), 2137-2184.
4. Morral, S. C. a. A. F. i., III-V Semiconductor Nanowire Solar Cells. In *Advances in III-V Semiconductor Nanowires and Nanodevices*, Jianye Li, D. W., Ray R. LaPierre, Ed. Bentham e-Books: 2011.
5. Saxena, D.; Mokkapati, S.; Parkinson, P.; Jiang, N.; Gao, Q.; Tan, H. H.; Jagadish, C. *Nat. Photonics* **2013,** 7, (12), 963-968.
6. Eshelby, J. D. *Journal of Applied Physics* **1953,** 24, (2), 176-179.
7. Roussel, J. M.; Gailhanou, M. *Phys. Rev. Lett.* **2015,** 115, (7).
8. Cao, A.; Wei, Y. G.; Ma, E. *Physical Review B* **2008,** 77, (19), 5.
9. Johansson, J.; Karlsson, L. S.; Svensson, C. P. T.; Martensson, T.; Wacaser, B. A.; Deppert, K.; Samuelson, L.; Seifert, W. *Nature Materials* **2006,** 5, (7), 574-580.
10. Utama, M. I. B.; de la Mata, M.; Magen, C.; Arbiol, J.; Xiong, Q. *Advanced Functional Materials* **2013,** 23, (13), 1636-1646.
11. Korgel, B. A. *Nature Materials* **2006,** 5, (7), 521-522.
12. Jacobsson, D.; Panciera, F.; Tersoff, J.; Reuter, M. C.; Lehmann, S.; Hofmann, S.; Dick, K. A.; Ross, F. M. *Nature* **2016,** 531, (7594), 317-322.
13. Holm, J. V.; Jorgensen, H. I.; Krogstrup, P.; Nygard, J.; Liu, H. Y.; Aagesen, M. *Nat. Commun.* **2013,** 4, 5.
14. Zhang, Y. Y.; Sanchez, A. M.; Wu, J.; Aagesen, M.; Holm, J. V.; Beanland, R.; Ward, T.; Liu, H. Y. *Nano Lett.* **2015,** 15, (5), 3128-3133.
15. Zhang, Y. Y.; Aagesen, M.; Holm, J. V.; Jorgensen, H. I.; Wu, J.; Liu, H. Y. *Nano Lett.* **2013,** 13, (8), 3897-3902.

16. Zhang, Y. Y.; Sanchez, A. M.; Sun, Y.; Wu, J.; Aagesen, M.; Huo, S. G.; Kim, D.; Jurczak, P.; Xu, X. L.; Liu, H. Y. *Nano Lett.* **2016,** 16, (2), 1237-1243.
17. Wu, J.; Li, Y. B.; Kubota, J.; Domen, K.; Aagesen, M.; Ward, T.; Sanchez, A.; Beanland, R.; Zhang, Y. Y.; Tang, M. C.; Hatch, S.; Seeds, A.; Liu, H. Y. *Nano Lett.* **2014,** 14, (4), 2013-2018.
18. Clark, S. J.; Segall, M. D.; Pickard, C. J.; Hasnip, P. J.; Probert, M. J.; Refson, K.; Payne, M. C. *Zeitschrift Fur Kristallographie* **2005,** 220, (5-6), 567-570.
19. Perdew, J. P.; Burke, K.; Ernzerhof, M. *Phys. Rev. Lett.* **1996,** 77, (18), 3865-3868.
20. Wen, C.-Y.; Reuter, M. C.; Bruley, J.; Tersoff, J.; Kodambaka, S.; Stach, E. A.; Ross, F. M. *Science* **2009,** 326, (5957), 1247-1250.
21. Holt, D. B. *Journal of Materials Science* **1966,** 1, 16.
22. Karlsson, L. S.; Dick, K. A.; Wagner, J. B.; Malm, J. O.; Deppert, K.; Samuelson, L.; Wallenberg, L. R. *Nanotechnology* **2007,** 18, (48).
23. Qian, X. F.; Kawai, M.; Goto, H.; Li, J. *Computational Materials Science* **2015,** 108, 258-263.
24. Brown, E.; Sheng, C. Y.; Shimamura, K.; Shimojo, F.; Nakano, A. *Journal of Applied Physics* **2015,** 117, (5).
25. Pond, R. C.; Vlachavas, D. S. *Proceedings of the Royal Society of London. A. Mathematical and Physical Sciences* **1983,** 386, (1790), 95-143.
26. Sawada, H.; Ichinose, H.; Kohyama, M. *Journal of Physics: Condensed Matter* **2007,** 19, (2), 026223.
27. Paxton, A. T.; Sutton, A. P. *Journal of Physics C: Solid State Physics* **1988,** 21, (15), L481.
28. Kohyama, M. *Modelling and Simulation in Materials Science and Engineering* **2002,** 10, (3), R31.
29. Sakaguchi, N.; Ichinose, H.; Watanabe, S. *Mater. Trans.* **2007,** 48, (10), 2585-2589.
30. Feng, C. B.; Nie, J. L.; Zu, X. T.; Al-Jassim, M. M.; Yan, Y. *Journal of Applied Physics* **2009,** 106, (11), 113506.
31. Cohen, D.; Carter, C. B. *Interface Science* **2003,** 11, (4), 391-401.
32. Feng, C. B.; Yin, W. J.; Nie, J. L.; Zu, X. T.; Huda, M. N.; Wei, S. H.; Al-Jassim, M. M.; Yon, Y. F. *Solid State Commun.* **2012,** 152, (18), 1744-1747.
33. Liu, C. Y.; Zhang, Y. Y.; Hou, Y. S.; Chen, S. Y.; Xiang, H. J.; Gong, X. G. *Physical Review B* **2016,** 93, (20).
34. Lazebnykh, V. Y.; Mysovsky, A. S. *Journal of Applied Physics* **2015,** 118, (13).
35. Sun Keun, C.; Minoru, M.; Toshiyuki, N. *Japanese Journal of Applied Physics* **1977,** 16, (5), 737.
36. Hohenberg, P.; Kohn, W. *Physical Review* **1964,** 136, (3B), B864-B871.
37. Kohn, W.; Sham, L. J. *Physical Review* **1965,** 140, (4A), A1133-A1138.
38. Mauger, A.; Bourgoin, J. C.; Allan, G.; Lannoo, M.; Bourret, A.; Billard, L. *Physical Review B* **1987,** 35, (3), 1267-1272.
39. Mirhosseini, H.; Kiss, J.; Felser, C. *Physical Review Applied* **2015,** 4, (6), 064005.
40. Tanaka, K.; Kohyama, M. *Philosophical Magazine A* **2002,** 82, (2), 215-229.
41. Wen, C. Y.; Tersoff, J.; Hillerich, K.; Reuter, M. C.; Park, J. H.; Kodambaka, S.; Stach, E. A.; Ross, F. M. *Phys. Rev. Lett.* **2011,** 107, (2), 025503.